Progress In Electromagnetics Research B, Vol. 23, 329–342, 2010

COMPARATIVE ANALYSIS BETWEEN EXPERIMENTAL CHARACTERIZATION RESULTS AND NUMERICAL FDTD MODELING OF SELF-ASSEMBLED PHOTONIC CRYSTALS

A. O. Silva

Electrical Engineering Department, EESC-USP
University of Sao Paulo
Sao Carlos, SP, Brazil

R. Bertholdo and M. G. Schiavetto

Institute of Chemistry, IQ-Unesp
Sao Paulo State University
Araraquara, SP, Brazil

B. V. Borges

Electrical Engineering Department, EESC-USP
University of Sao Paulo
Sao Carlos, SP, Brazil

S. J. L. Ribeiro and Y. Messaddeq

Institute of Chemistry, IQ-Unesp
Sao Paulo State University
Araraquara, SP, Brazil

M. A. Romero

Electrical Engineering Department, EESC-USP
University of Sao Paulo
Sao Carlos, SP, Brazil

Received 4 June 2010, Accepted 19 July 2010, Scheduled 25 July 2010
Corresponding author: M. A. Romero (murilo.romero@usp.br).

Abstract—This paper presents a comparative analysis between the experimental characterization and the numerical simulation results for a three-dimensional FCC photonic crystal (PhC) based on a self-assembly synthesis of monodispersive latex spheres. Specifically, experimental optical characterization, by means of reflectance measurements under variable angles over the lattice plane family $[1, 1, 1]$, are compared to theoretical calculations based on the Finite Difference Time Domain (FDTD) method, in order to investigate the correlation between theoretical predictions and experimental data. The goal is to highlight the influence of crystal defects on the achieved performance.

1. INTRODUCTION

The propagation of electromagnetic waves through structures displaying periodic variations of refractive index presents a close analogy with solid-state physics, where the periodicity of the crystalline lattice is responsible for the rising of a discrete set of allowed energy bands and gaps. Similarly, the behavior of an electromagnetic wave propagating through a periodic medium will exhibit allowed and forbidden modes. Structures presenting such properties in micrometer/nanometer scales are called photonic crystals (PhCs) and represent a family of optical devices offering both low loss and high optical confinement. Many applications in optoelectronics are expected from photonic crystals, including ultra small optical circuits, resonators, filters and lasers [1, 2].

Since the 90's major efforts into obtaining full three-dimensional photonic crystals have been made. The main difficulty lies on the fabrication method, which should assure a high degree of precision. In this context, three approaches stand out. The first consists on the repeated application of planar lithographic methods in a layer-by-layer sequence [3], by means of a serial writing process where the patterns of each layer are drawn sequentially. This technique is compatible with CMOS microelectronics infrastructure but requires high cost processing equipment. It is also slow and involves the difficulty of precisely alignment for lithography and etching steps in a nanometer scale.

A second approach uses volumetric patterning of photosensitive materials to create a template structure [4]. The method involves two basic strategies, namely, serial writing and parallel holography. The first uses a tightly focused ultra-fast IR laser and multi photon absorption to carry out the photopolymerization of a resist on a point-

by point basis. By its turn, parallel holography is the 3D generalization of the 2D holographic method and involves the interference of coherent laser beams within the resist material to form a 3D interference pattern, which can be designed to match a desired photonic crystal lattice.

Finally, a third popular approach involves the self-assembly of particle dispersions to form templates which are subsequently back-filled with a desired material [5]. The resultant structures are called artificial opals since they are analogous to natural opal stones but fabricated in laboratory, under controlled conditions. The advantages are low cost and high speed, as the self-assembly is a parallel process.

The development of algorithms to simulate electromagnetic wave propagation in 3D PhCs is another crucial challenge. A suitable simulation technique must be able to accurately compute the electromagnetic response in a broad spectral range. The Finite Difference Time Domain Method (FDTD) [6] meets such requirement and it is widely used to analyze PhCs [7]. The method is based on directly solving the finite-difference form of Maxwell equations to calculate electromagnetic fields propagating through a given medium.

In the last few years, the application of the FDTD method to the modeling of PhCs has been carried out by a large number of research groups. Unfortunately, the basic FDTD implementation requires intense computational effort, which has generally limited its application to 2D PhC geometries. Only recently, advances in computational power and architecture allowed the extension of the FDTD method to full three dimensional PhC analysis [8]. As a consequence, most numerical studies have focused on 2D PhC slabs, as it is well depicted in [9–12]. In these previous investigations, although the 3D-FDTD method is employed in order to account for the finite thickness of the crystal thickness, the simulated crystal lattice still displays a two-dimensional periodicity.

In the above framework, our work revisits the fabrication, optical characterization and numerical modeling of a photonic crystal based on a self-assembly synthesis. We seek to explore the interplay between theory and experiment, since all parameters concerning the numerical simulation and PhC fabrication are under our direct control. To this aim a FDTD implementation taking into account the three-dimensional periodicity of the PhC crystal lattice was implemented. An additional bonus of the overall procedure is to enable the developed algorithm as an appropriate simulation tool for future optimization of the fabricated crystal.

The paper deeply extends some of our previous results [13] and it organized as follows. The fabrication method for our PhC, composed of

latex opals embedded in air and structured in a FCC (face-centered-cubic) arrangement, is described in Section 2. Compared to higher refractive index materials, the use of latex spheres usually allows improved process control, which is very convenient for the purposes of the present study. Section 3 is devoted to present the 3D FDTD algorithm and to discuss the calculated PhC bandstructure. It is demonstrated that, on account of the low refractive index between latex and air, a full photonic band gap (PBG) is not possible. Still, in Section 4, reflectance spectroscopy results for the crystal are presented to indicate the existence of a clear Bragg diffraction pattern, associated to the rising of photonic gaps along certain directions of propagation. Finally, in Section 5, a detailed comparison between the experimental results and FDTD numerical predictions is carried out to allow a full understanding of our findings.

2. FABRICATION OF LATEX-OPAL BASED 3D PHOTONIC CRYSTAL

Natural opals are silica-based materials where monodispersed submicrometer amorphous silica spheres, with chemically bonded water molecules, are spontaneously arranged in a periodic structure. The mesoscale structure within the mineral causes Bragg diffraction of light producing the optical effects displayed by these materials. Synthetic opals can be prepared from monodispersive latex spheres, among a range of other possible materials.

Our latex spheres have been synthesized according to a single-stage polymerization process based on formation and growth of polymeric nuclei dispersed in a water-styrene-potassium persulfate emulsion [14]. Synthesis began with introduction of 1700 mL of water and 200 mL of styrene (Merck) under continuous stirring into a 5 L round glass bottle. Three parameters have been controlled during the synthesis: temperature, impeller speed, and initiator addition. Temperature was kept at $70 \pm 2°C$ along the emulsion through a thermal bath. A mechanical stirrer controlled impeller speed with a variation estimated at 1 rpm. The initiator is constituted by 100 mL of a $2.45 \times 10^{-2}\,\mathrm{mol} \cdot \mathrm{L}^{-1}$ aqueous solution of potassium persulfate (Mallinckrodt) whose addition in the emulsion was performed by a peristaltic pump for 24 h (0.07 mL/min). Emulsion has been kept under continuous stirring for 4 h after complete addition of the initiator. The four synthesized samples reveal a spherical homogeneous shape by TEM measurements. The diameter-size of the latex spheres samples synthesized with impeller speed of emulsion at 250, 300, 350 and 400 rpm were 281 nm (CV value of 3.9), 294 nm (CV 1.7), 619 nm

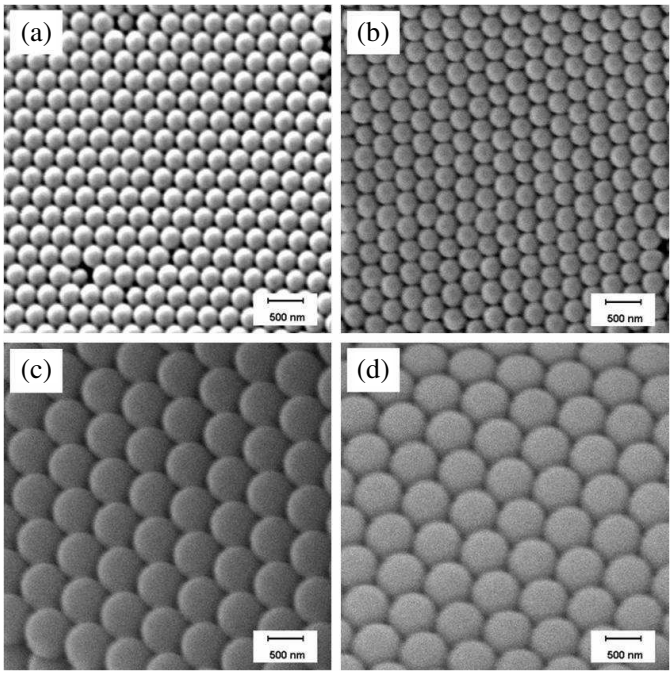

Figure 1. Representative SEM images of the $[1, 1, 1]$ plane of the 3D photonic crystal for all four samples described above, obtained at 250, 300, 350 and 400 rpm, respectively (latex-250, latex-300, latex-350, latex-400, clockwise, from (a) to (d)).

(CV 1.9) and 687 nm (CV 1.6), respectively. In the present case, the coefficient of variation (CV) is a statistical measure of the size dispersion on a given population of latex spheres. Specifically, the CV parameter is calculated as the ratio between the standard deviation (σ) and the average size (μ) of the spheres.

The increase in sphere size as the impeller speed raise occurs due to the enhancement of the coagulation process which takes place during the synthesis of the latex spheres. Specifically, the size increase for latex spheres synthesized at high impeller speed is attributed to a change in the mixing entropy of the emulsion, resulting in a more intense aggregation of the colloidal particles. The coagulation process becomes stronger above 300 rpm and it is the reason why the sphere diameter doubles as the speed is raised from 300 rpm to 350 rpm.

The latex opals films were achieved by a controlled water evaporation method [15]. 7.5×1.25 cm substrates were cut from microscope slides and cleaned by sequential washing with 3 : 1

H_2SO_4 : 30% H_2O_2 (80°C, 1 h), deionized water, 5 : 1 : 1 H_2O : NH_4 : 30% H_2O_2 (ultrasonic bath, 1 h), deionized water and finally nitrogen stream. Cleaned hydrophilic substrates were vertically positioned in the center of 10 mL polyethylene cylindrical vials containing around 7 mL of latex colloidal suspension. The vials were placed into a controlled temperature chamber at 50°C. After the complete water evaporation, the resulting colloidal crystals were completely dried under vacuum at 70°C for 3 h. Fig. 1 shows representative SEM images from the frontal face (the $[1, 1, 1]$ plane) of the opal based photonic crystal for all four samples described above, obtained at 250, 300, 350 and 400 rpm, respectively (latex-250, latex-300, latex-350, latex-400, clockwise, from (a) to (d)).

SEM characterization confirms that the opal-based PhC has crystallographic domains extending over the micrometric range, but with a few localized defects. In order present our FDTD formulation and to gain insight on the allowed and forbidden modes corresponding to the latex-opal based PhC, the following section is devoted to obtain and discuss the bandstructure of an ideal FCC crystal.

3. LATEX-OPAL BASED PHC BANDSTRUCTURE

The bandstructure calculation of the latex-opal based PhC is carried out by the FDTD method [6]. In this initial simulation, we assumed an ideal FCC lattice, although the finite thickness of the PhC is taken into account. The influence of localized defects is discussed in the next sections.

The FDTD calculation of the crystal bandstructure was performed using a superposition of planes waves acting as the optical excitation [16]. This optical excitation scans the irreducible Brillouin zone of the crystalline lattice in order to yield a complete description of the allowed and forbidden frequencies for all directions of propagation. The optical source is expressed by the phasor electric field component E_y in (1), where $\bar{G}$ is the reciprocal lattice vector, $\bar{r}$ is the direct lattice vector and E° is the field amplitude. The spatial increments and indexes are denoted by Δx, Δy, Δz, i, l and k, respectively.

$$E_y(i\Delta x,\, l\Delta y,\, k\Delta z) = \sum_{\bar{G}} E^o \exp\left[j\left(\bar{k} + \bar{G}\right)\bar{r}\right] \tag{1}$$

A realistic calculation of the crystal bandstructure must consider a finite thickness. This need is well accounted for by the FDTD method. However, the high computational cost required implies in an extremely time-consuming algorithm. To overcome this difficulty, the present modeling considers the crystal finite only along the

longitudinal direction. In the FDTD simulations we assumed a FCC crystal structure and typically took into account 5 lattice constants in the longitudinal direction. The PML (perfectly matched layer) boundary condition [17] is used to model the longitudinal terminations of the computational domain. On the other hand, as the crystal is taken as infinite in the transversal directions, the respective domain terminations are modeled by periodic boundary condition [6].

In principle, the bandstructure is obtained applying Fourier transform to the time-sequence of one field component at one space point. The eigenfrequencies are the ones corresponding to the peaks of the amplitude spectrum for each wavevector of the irreducible Brillouin zone. However, in practice, this is an inaccurate procedure because the chosen field component can be zero at this particular point. Consequently, this mode can be missed in the final spectrum. Instead, our FDTD algorithm uses ten test points randomly chosen on the staggered grid in order to determine the eigenfrequencies. Then, the required Fourier transform is directly obtained by a DFT (discrete Fourier transform) algorithm performed after the FDTD calculations.

The computational infrastructure used to run the FDTD algorithm consists of a cluster composed by twenty four processors of 2.8 GHz, equally distributed among twelve nodes. Each node has 2 GB of memory RAM. Working as a parallel engine, each node was responsible for calculating the eigenfrequencies of one wavevector of the irreducible Brilouin zone.

The resulting bandstructure average latex-opal based PhC (opal

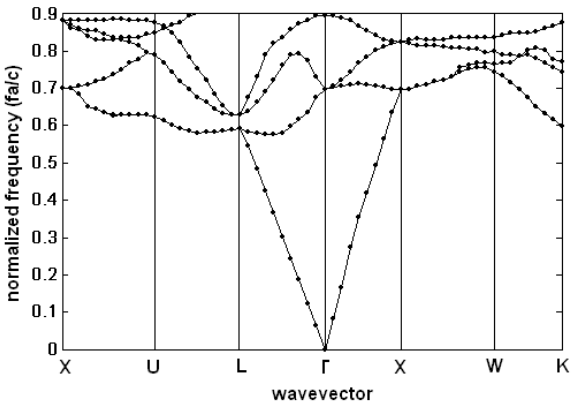

Figure 2. Bandstructure of the 3D latex-opal based photonic crystal. The average opal diameter corresponds to the sample obtained at 300 rpm (latex-300).

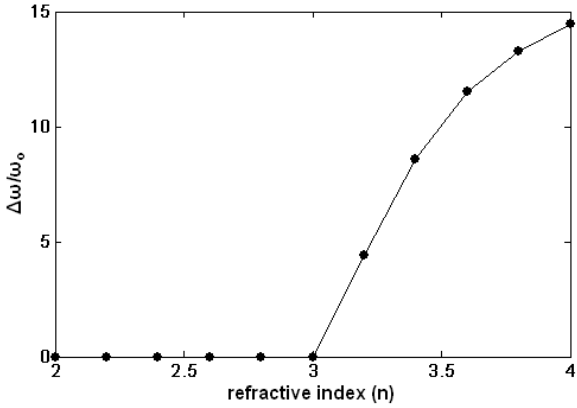

Figure 3. Photonic gap width as a function of the refraction index for our FCC opal based crystals; ω_o is the central frequency of the gap.

diameter of about 300 nm) is presented in Fig. 2. The bands fully overlap for all values of wavevector in k-space. Thus, no bandgap is found. To understand the influence of the refractive index n on the photonic bandgap opening in our FCC opal-based PhC, the FDTD algorithm was used to calculate the variation of the relative band gap width as the refractive index n is increased. The relative bandgap was computed between the first and second bands in the **X** direction (see Fig. 2) and the opals are supposed embedded in air. The X direction was selected because it allows significant bandgap changes as the refractive index is raised. The obtained diagram is presented in Fig. 3. A photonic gap arises only for refractive indexes larger then 3.0.

However, although there is no a full PBG in the bandstructure of the latex-opal based PhC, forbidden spectral ranges in certain directions of propagation can be observed. For instance, there is a photonic gap comprising the normalized spectral range $[0.7, 0.9]$ along the **Γ** direction. The presence of these photonic gaps is associated to Bragg diffraction phenomenon and, consequently, allows to check how well ordered the opals are in the crystalline lattice. The experimental investigation of Bragg diffraction pattern related to the latex-opal based PhC is the subject of the following section.

4. REFLECTANCE MEASUREMENTS ASSOCIATED TO THE LATEX-OPAL BASED PHC

The optical characterization of PhCs by reflectance spectra is an accurate way to check the quality of the crystalline samples. When an optical beam with is normally focused into the crystal, the rising of a reflection band indicates the existence of a crystalline plane. As the angle of incidence is varied, a Bragg diffraction pattern can be obtained corresponding to the variation of the Bragg wavelength λ_M. As a consequence, the interplanar distance d_{hkl} can be related to the angle of incidence through the Bragg relationship, as follows [18]:

$$\lambda_M = \frac{2d_{hkl}}{m}\sqrt{n_{eff}^2 - \sin^2\theta} \tag{2}$$

where m is the diffraction order, which is supposed 1.0 in our work, and θ is the angle of incidence measured from the normal to the crystalline planes. In a first approximation, the effective refractive index n_{eff} can be taken as:

$$n_{eff} = n_{mat.}f + n_{air}(1-f) \tag{3}$$

where n_{mat} is the refractive index of latex (1.59 at the red wavelength), n_{air} is the refractive index of free space (1.0) and f is the filling factor. Regarding the numerical simulations, the full spectral dependence of the latex refractive index is described accordingly to reference [19]. The optical losses were not taken into account in the formulation.

We carried out the optical characterization of our samples by variable angle specular reflectance (VASR) related to the [111] crystalline planes in a Cary 500 (VARIAN) spectrophotometer. The 2–16° spectra were obtained in a homemade setup and the 20–50° spectra with an original VASR accessory.

Figure 4 shows the representative experimental results obtained for distinct angles of incidence to sample latex-400 (see Section 2). As expected from Eq. (2), there is a progressive shift of the reflection peak towards lower wavelengths as the angle of incidence is increased. In order to obtain the filling factor of each PhC sample, a linear fit between the experimental values of λ_M and the values calculated from (2) was performed. The fitted results to all crystalline samples range from 73% (latex-250 and latex-300, corresponding opal diameter of 290 and 303 nm, respectively) down to 59% (latex-350, corresponding opal diameter of 630 nm) and 54% (latex-400, corresponding opal diameter of 685 nm).

The variation of Bragg wavelength as a function of the angle of incidence was next obtained by the FDTD algorithm. The following section is devoted to a comparative analysis between the experimental results and FDTD numerical predictions.

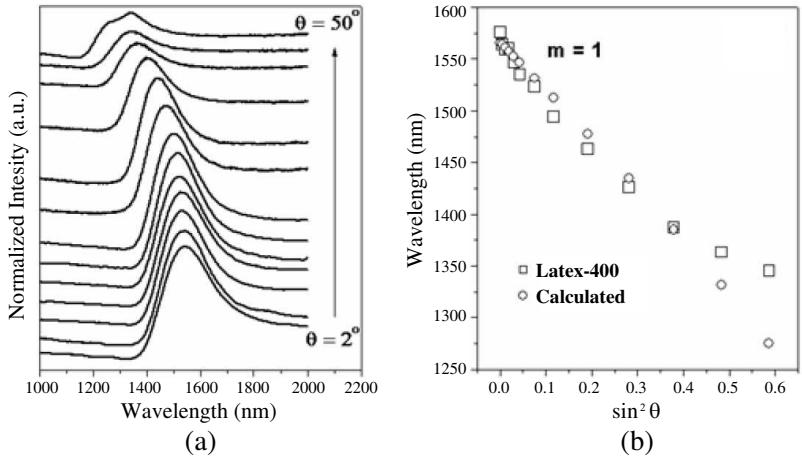

Figure 4. Representative results for the latex-400 sample. (a) Specular reflectance spectra obtained from distinct angles of incidence, (b) linear fit between the experimental values of λ_M and the values calculated from Eq. (2).

5. CALCULATION OF BRAGG WAVELENGTH AS FUNCTION OF THE ANGLE OF INCIDENCE

To compute the Bragg wavelength as the angle of incidence is varied, the FDTD modeling considered FCC lattices with the values of opal diameter and filling factor experimentally obtained in the previous section. Fig. 5 depicts the experimental results and FDTD calculations of Bragg wavelength as function of $\sin^2\theta$ for the fabricated opal-based PhCs. The FDTD results are in good agreement with the experimental values of Bragg wavelength for low angles of incidence. However, there is an appreciable divergence for $\sin^2\theta > 0.3$. Several causes may contribute to this behavior. Among those, we mention the disorder defects in the PhC samples. In fact, as a result of lattice defects, it is expected that the interplanar distance will randomly vary around the nominal value, causing a deviation of the expected Bragg wavelength [20].

Unfortunately, even using the computer cluster described in Section 3, the computational effort to include random defects in a FDTD PhC simulation was still too intense to be meaningful. As an alternative, for sample latex-300, Fig. 5(b), we numerically calculated the change in the Bragg wavelength as the distance d_{111} is increased, for a typical incidence angle of 38°, an incidence angle for which theory

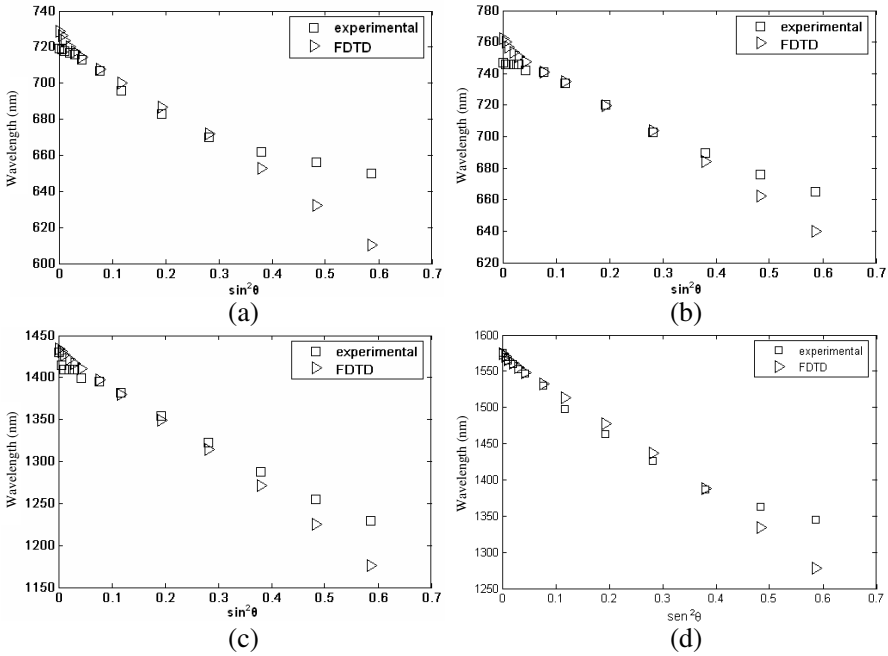

Figure 5. Experimental and FDTD results for Bragg wavelength as a function of the incidence angle, from top to bottom. (a) latex-250, (b) latex-300, (c) latex-350 and (d) latex-400. The larger size of the spheres for samples latex-350 and latex-400 samples shifts the Bragg wavelength from the visible into the infrared range.

and experiment start to significantly depart. The goal was to verify if a small change in the expected interplanar distance would significantly move the Bragg wavelength away from the ideal case, depicted by the theoretical results of Fig. 5. For instance, consistently with the experimental data of Fig. 5(b), Fig. 6 indicates that an increase of 5% in the value of d_{111} causes a Bragg wavelength shift of about 25 nm, from around 685 nm up to close of 710 nm.

To further discuss the experimental data, the behavior of the full width at half maximum (FWHM) of the reflectance spectra was also investigated. To highlight this issue, the calculated dependence of the FWHM of these spectra as function of the angle of incidence is presented in Fig. 7, where the results obtained by the FDTD algorithm considering the well-structured FCC sample latex-300. Our simulations suggest that these results, displaying a clear broadening of the FWHM beyond 20 degrees of incidence, are mostly caused by

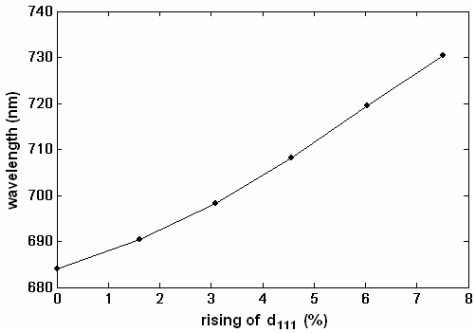

Figure 6. Variation of Bragg wavelength with the rising of d_{111}.

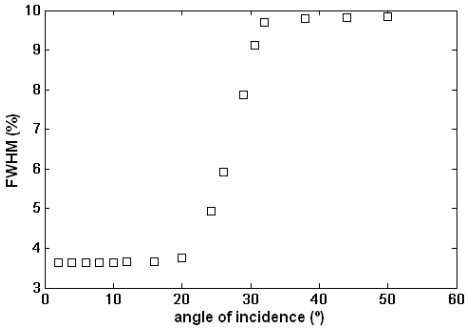

Figure 7. Calculated FWHM as function of the angle of incidence for the sample latex-300. The percentage value is taken from the peak wavelength.

a superposition of distinct Bragg peaks, arising from simultaneous reflections from adjacent crystal planes, as previously discussed in [21].

6. CONCLUSIONS

We reported a self-assembly synthesis technique for fabricating a latex-opal based full 3-D photonic crystal. The experimental optical characterization of the PhC structure was performed by measurements of specular reflectance on the [111] family of planes for incidence angle and showed a clear Bragg diffraction signature despite the presence of localized defects through the crystal lattice. Further insight was gained by application of the FDTD method to theoretically investigate the PhC band structure. As expected the crystal presented an incomplete photonic band gap, on account of the relatively low refractive index

contrast between air and latex. Correlation between the FDTD simulations and the experimental data suggest that disorder defects are responsible for the discrepancies between theory and experiment for large incidence angles. Also, the FWHM broadening beyond 20 degrees of incidence was shown to be possibly caused by a superposition of distinct Bragg peaks, arising from simultaneous reflections from adjacent crystal planes. However, further investigation is needed to clarify this issue.

REFERENCES

1. Joannopoulos, J. D., R. D. Meade, and J. N. Winn, *Photonic Crystals: Molding the Flow of Light*, Princeton University Press, Princeton, NJ, 1995.
2. Wu, C. J., J. J. Liao, and T. W. Chang, "Tunable multilayer fabry-perot resonator using electro-optical defect layer," *Journal of Electromagnetic Waves and Applications*, Vol. 24, No. 4, 531–542, 2010.
3. Johnson, S. G. and J. D. Joannopoulos, "Three-dimensionally periodic dielectric layered structure with omnidirectional photonic band gap," *Applied Physics Letters*, Vol. 77, No. 22, 3490–3492, 2000.
4. Sun, H. B., S. Matsuo, and H. Misawa, "Three-dimensional photonic crystal structures achieved with two-photon-absorption photopolymerization of resin," *Applied Physics Letters*, Vol. 74, No. 6, 786–788, 1999.
5. Xia, Y., B. Gates, and Z.-Y. Li, "Self-assembly approaches to three-dimensional photonic crystals," *Advanced Materials*, Vol. 13, No. 6, 371–375, 2001.
6. Taflove, A. and S. Hagness, *Computational Electrodynamics: The Finite-difference Time-domain Method*, Artech House, Boston, 2005.
7. Chan, C. T., Q. L. Yu, and K. M. Ho, "Order-N spectral method for electromagnetic waves," *Phys. Review B*, Vol. 51, 16635–16642, 1995.
8. Hermann, C. and O. Hess, "Modified spontaneous emission rate in an inverse opal structure with complete photonic band gap," *Journal of Optical Society of America B*, Vol. 19, No. 12, 3013–3018, 2002.
9. Davanço, M., A. Xing, J. W. Raring, E. L. Hu, and D. J. Blumenthal, "Compact broadband photonic crystal filters with reduced back-reflections for monolithic InP-based photonic

integrated circuits," *IEEE Photonics Technology Letters*, Vol. 18, No. 10, 1155–1157, 2006.

10. Skivesen, N., A. Têtu, and M. Kristensen, "Photonic crystal waveguide biosensor," *Optics Express*, Vol. 15, No. 6, 3169–3176, 2007.
11. Faraon, A., E. Waks, D. Englund, I. Fushman, and J. Vuckoic, "Efficient photonic crystal cavity-waveguide couplers," *Applied Physics Letters*, Vol. 90, 1–3, 2007.
12. Lee, M. and P. M. Fauchet, "Two-dimensional silicon photonic crystal based biosensing platform for protein detection," *Optics Express*, Vol. 15, No. 8, 4530–4535, 2007.
13. Bertholdo, R., A. O. Silva, M. G. Schiavetto, B. H. V. Borges, S. J. L. Ribeiro, Y. Messaddeq, and M. A. Romero, "Fabrication and analysis of self-assembled photonic crystals structures," *Proceedings of the SBMO/IEEE MTT-S International Microwaves and Optoelectronics Conference*, Vol. 1, 50–53, 2007.
14. Alencar, M. A., G. S. Maciel, C. B. Araújo, R. Bertholdo, Y. Messaddeq, and S. J. Ribeiro, "Laserlike emission from silica inverse opals infiltrated with Rhodamine 6G," *Journal of Non-Crystalline Solids*, Vol. 351, 1846–1849, 2005.
15. Wong, S., V. Kitaev, and G. A. Ozin, "Colloidal crystal films: advances in universality and perfection," *Journal of the American Chemical Society*, Vol. 125, No. 50, 15589–15598, 2003.
16. Ho, K. M., C. T. Chan, and C. M. Soukoulis, "Existence of a photonic gap in periodic dielectric structures," *Physical Review Letters*, Vol. 65, No. 25, 3152–3155, 1990.
17. Berenger, J. P., "Three-dimensional perfectly matched layer absorbing medium for the truncation of FDTD lattices," *Journal of Computational Physics*, Vol. 127, No. 0181, 363–379, 1995.
18. Bohren, C. F. and D. Huffman, *Absorption and Scattering of Light by Small Particles*, John Wiley and Sons, New York, 1983.
19. Kasarova, S. N., N. G. Sultanova, S. D. Ivanov, and I. D. Nikolov, "Analysis of the dispersion of optical plastic materials," *Optical Materials*, Vol. 29, 1481–1490, 2007.
20. Mayoral, R., J. Requena, J. S. Moya, C. Lopez, A. Cintas, H. Miguez, F. Meseguer, L. Vazquez, M. Holgado, and A. Blanco, "3D long-range ordering in an SiO_2 submicrometer-sphere sintered superstructure," *Advanced Materials*, Vol. 9, 257–260, 1997.
21. Martinez, J. M., "Modeling of opal-based photonic crystals," Ph.D. Thesis, Université Montpellier, 2002 (in French).